ACS APPLIED MATERIALS & INTERFACES

Research Article

www.acsami.org

PEGylated Artificial Antibodies: Plasmonic Biosensors with Improved Selectivity

Jingyi Luan,[†] Keng-Ku Liu,[†] Sirimuvva Tadepalli,[†] Qisheng Jiang,[†] Jeremiah J. Morrissey,[‡,§] Evan D. Kharasch,[‡,§,∥,⊥] and Srikanth Singamaneni*[,†,§]

[†]Department of Mechanical Engineering and Materials Science, Institute of Materials Science and Engineering, Washington University in St. Louis, St Louis, Missouri 63130, United States

[‡]Department of Anesthesiology, Washington University in St. Louis, St. Louis, Missouri 63110, United States

[§]Siteman Cancer Center, [∥]Department of Biochemistry and Molecular Biophysics, Washington University in St. Louis, St. Louis, Missouri 63110, United States

[⊥]The Center for Clinical Pharmacology, St. Louis College of Pharmacy and Washington University School of Medicine, St. Louis, Missouri 63110, United States

Supporting Information

ABSTRACT: Molecular imprinting, which involves the formation of artificial recognition elements or cavities with complementary shape and chemical functionality to the target species, is a powerful method to overcome a number of limitations associated with natural antibodies. An important but often overlooked consideration in the design of artificial biorecognition elements based on molecular imprinting is the nonspecific binding of interfering species to noncavity regions of the imprinted polymer. Here, we demonstrate a universal method, namely, PEGylation of the noncavity regions of the imprinted polymer, to minimize the nonspecific binding and significantly enhance the selectivity of the molecular imprinted polymer for the target biomolecules. The nonspecific binding, as quantified by the localized surface plasmon resonance shift of imprinted plasmonic nanorattles upon exposure to common interfering proteins, was found to be more than 10 times lower compared to the non-PEGylated counterparts. The method demonstrated here can be broadly applied to a wide variety of functional monomers employed for molecular imprinting. The significantly higher selectivity of PEGylated molecular imprints takes biosensors based on these artificial biorecognition elements closer to real-world applications.

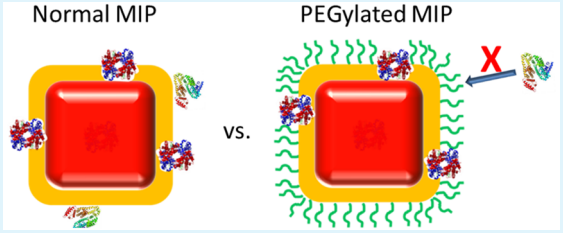

KEYWORDS: *PEGylation, artificial antibody, molecular imprinting, plasmonic biosensor, localized surface plasmon resonance*

1. INTRODUCTION

Antibody−antigen interactions form the basis for numerous bioassays, such as enzyme-linked immunosorbent assay (ELISA), Western blotting, and immunoprecipitation assay.[1,2] Although natural receptors (e.g., monoclonal antibodies) have excellent molecular recognition capabilities, their biological origin imposes several inherent limitations, such as (i) limited pH and temperature stability; (ii) loss of conformation and recognition functionality in nonaqueous media; (iii) high cost associated with raising and harvesting natural antibodies; and (iv) poor compatibility with micro and nanofabrication processes for efficient integration with various transduction platforms. These issues impose severe challenges in the translation of a number of biodiagnostic platforms to point-of-care and resource-limited settings.[3,4] Localized surface plasmon resonance (LSPR) wavelength of metal nanostructures is highly sensitive to the changes in the refractive index of the surrounding medium.[5,6] Label-free biosensing platforms based on refractive index sensitivity of LSPR wavelength hold enormous potential to provide highly sensitive, cost-effective, on-chip, and point-of-care diagnostic tools.[7−9] However, most of the existing LSPR biosensors also rely on natural antibodies as biorecognition elements, making them prone to the above-mentioned limitations.

Synthetic biorecognition elements or artificial antibodies based on molecular imprinting, which exhibit remarkable stability over a wide range of conditions (e.g., pH, temperature, solvent) are an attractive alternative to natural receptors.[10−16] Artificial antibodies based on molecular imprinting are produced by creating "binding or recognition sites" in a polymer network using target (bio)molecules as templates. The binding sites are achieved by (co)polymerizing and cross-linking functional monomers around the template species. The template is subsequently removed by cleaving a predesigned reversible bond between the biomolecular template and the substrate. Upon removal of the template species, the polymer is left with cavities (i.e., binding sites), which are complementary in size, shape, and chemical functionality to the template

Received: June 15, 2016
Accepted: August 19, 2016

DOI: 10.1021/acsami.6b07252
ACS Appl. Mater. Interfaces XXXX, XXX, XXX−XXX

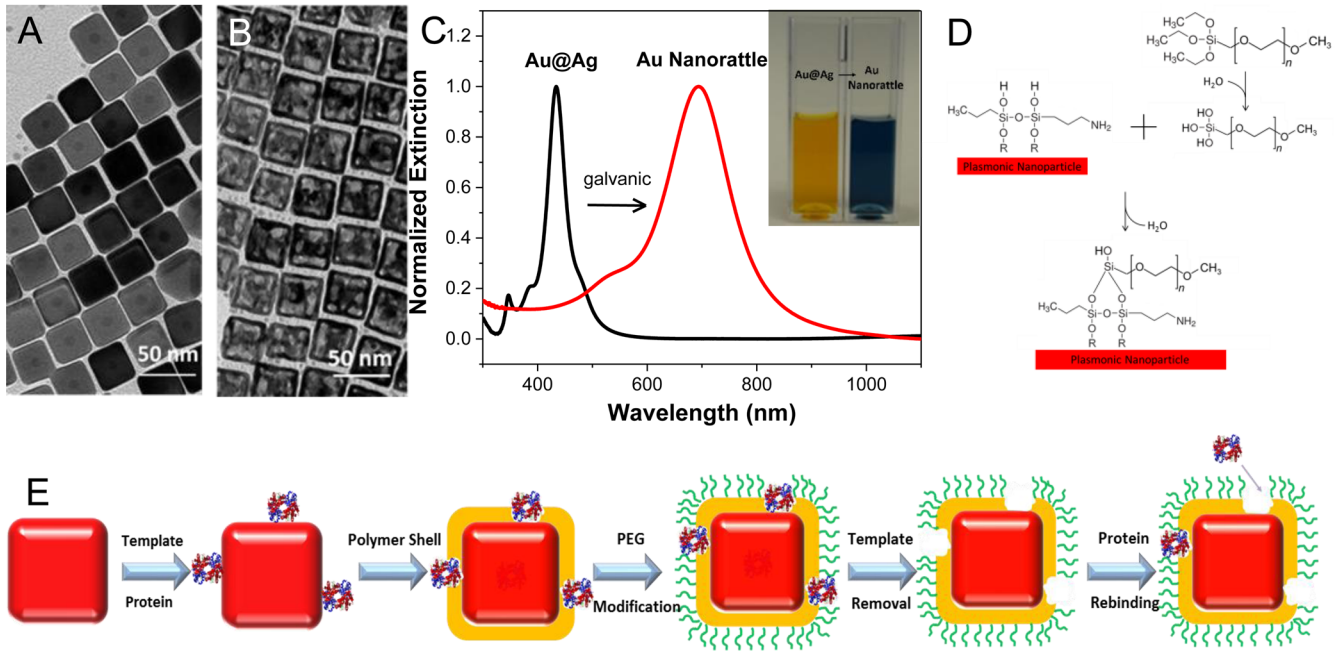

Figure 1. TEM image of (A) Au@Ag nanocubes and (B) Au nanorattles. (C) Vis-NIR extinction spectra of aqueous suspension of Au@Ag nanocubes and Au nanorattles. Inset shows the photographs of the corresponding aqueous solutions. (D) Schematic illustration of the chemical grafting of PEG chains to the siloxane copolymer surface. (E) Schematic illustration showing the various steps involved in the formation and PEGylation of the artificial antibodies.

species. The imprinted binding sites can then be accessed by target analytes with the same size, shape, and chemical functionality as the template species. Recently, we have demonstrated plasmonic biosensors based on artificial antibodies using gold nanorods and nanocages as plasmonic nanotransducers.[17,18]

The sensitive (high binding affinity) and selective binding of the target molecules to the artificial receptor are the two most important criteria in creating an artificial antibody.[19,20] A number of studies have focused on improving the binding affinity of the artificial antibodies through rational choice of the functional monomers and optimizing the polymerization conditions.[21,22] Yet another important factor that needs to be carefully considered in the design of artificial antibody-based biosensors is the nonspecific binding of interfering species, which increases the noise floor of the biosensor and compromises the limit of detection. There have been only a few studies that focus on reducing the effect of nonspecific binding by epitope imprinting or second polymerization.[23,24] However, these methods are specific to the application and impose restrictions on the target protein or the polymerization material.

Polyethylene glycol (PEG) is a highly flexible hydrophilic polymer that is extensively used in biology and life sciences as a blocking agent to resist nonspecific adsorption of proteins on implant surfaces and nanoparticles intended for biodetection, therapy, and imaging.[25,26] The protein-repelling effect of PEG owes to the low free energy at PEG−water interface, absence of hydrogen bonding and electrostatic interactions with proteins, and the high flexibility of PEG chains.[27] Although intensively studied and frequently used, to the best of our knowledge, there is no report describing the use of PEG in molecular imprinting to block the nonspecific interaction. Here, we introduce a universal approach to minimize nonspecific binding by blocking the nonrecognition regions of the imprinted polymer with PEG before removing the template biomolecules. Successful grafting of the PEG chains on the surface of siloxane copolymer was confirmed using a series of surface characterization techniques. We demonstrate that PEG chains grafted to the noncavity regions of imprinted polymer can greatly lower the nonspecific binding of interfering proteins without perturbing the selectivity of the imprinted polymers.

2. RESULTS AND DISCUSSION

Hollow plasmonic nanostructures, such as Au nanoshells, nanocages, nanoframes, and nanorattles, exhibit significantly higher refractive index sensitivity compared to their solid counterparts, making them excellent choices as nanotransducers for plasmonic biosensors.[28] In this study, we have employed Au nanorattles (AuNRT) comprised of Au nanoparticle core and cubic and porous Au shell as nanotransducers and hemoglobin (Hb) employed as a model protein, which is the disease biomarker for hemoglobinuria. Hemoglobinuria occurs under a number of urinary tract cancers, such as kidney, bladder, or prostate cancers,[29] and a wide variety of noncancerous renal diseases, including, but not limited to, hemolytic uremic syndrome[30] and paroxysmal nocturnal hemoglobinuria.[31] The concentration of hemoglobin in urine under pathological conditions can reach 600 ng/mL or more.[32] Realization of AuNRTs starts with synthesis of Au nanospheres (AuNS), which serve as seeds for Au@Ag nanocubes. AuNS were, in turn, synthesized using a seed-mediated method (see experimental section for details).[33] Transmission electron microscopy (TEM) images revealed the narrow size distribution of AuNS with a diameter of 8.5 ± 0.6 nm (see SI, Figure S1). The Au@Ag nanocubes also exhibited a narrow size distribution with an edge length of 31.0 ± 1.1 nm (n > 50). The AuNS cores were found to be at the center of each Au@Ag nanocube indicating the uniform overgrowth of Ag on the surface of the AuNS (Figure 1A). The AuNS@Ag nanocubes

DOI: 10.1021/acsami.6b07252
ACS Appl. Mater. Interfaces XXXX, XXX, XXX−XXX

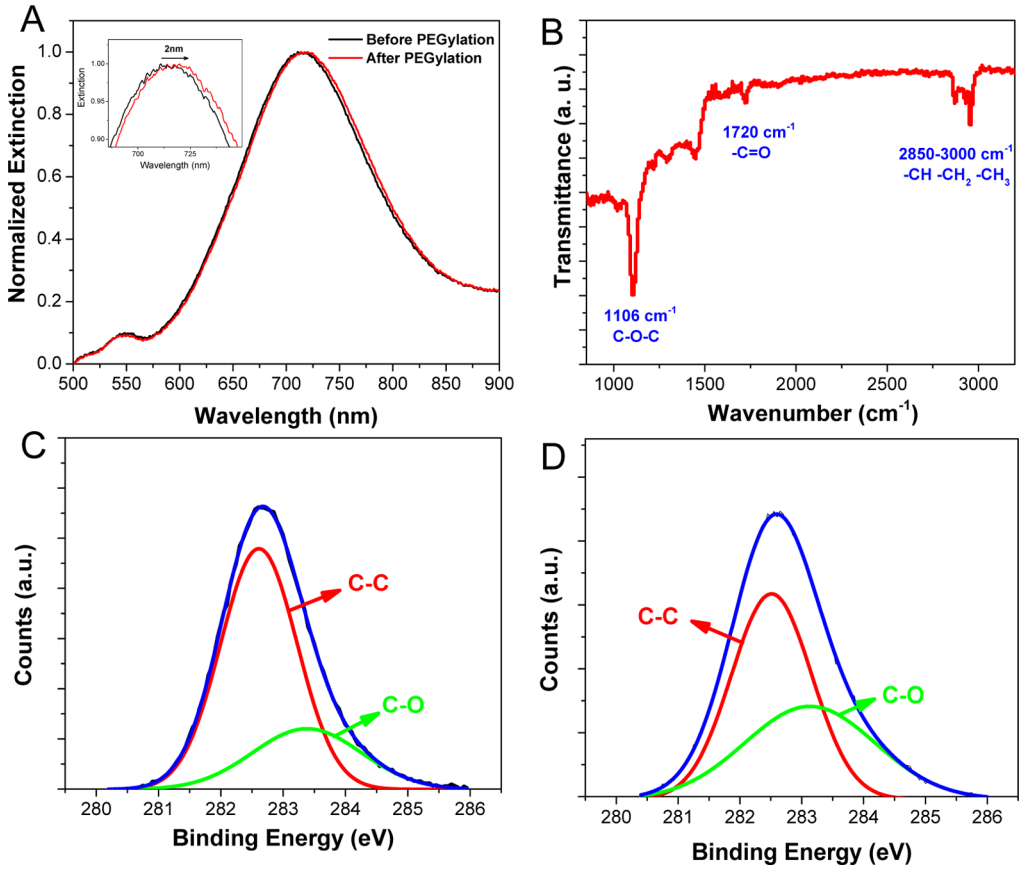

Figure 2. (A) Extinction spectra of AuNRT before and after PEGylation of the siloxane copolymer surface (zoomed-in plot in the inset shows the ~2 nm red shift). (B) FTIR spectrum after PEGylation of the siloxane copolymer showing the characteristic bands corresponding to PEG. X-ray photoelectron spectra (C) before and (D) after PEGylation of the siloxane copolymer surface showing the dramatic increase in the C−O/C-C intensity ratio from 0.36 to 0.68.

are dominated (100) facets due to the faster growth of Ag on the (111) facets of cuboctahedral Au nanoparticles.[34] Galvanic replacement reaction is an electrochemical reaction which involves the oxidation of one metal with lower reduction potential (which serves as a sacrificial template) by the ions of another metal with higher reduction potential.[35] We employed galvanic replacement reaction to synthesize AuNRT using Au@Ag nanocubes as templates. Addition of $HAuCl_4$ to Au@Ag nanocubes solution resulted in spontaneous galvanic replacement reaction and formation of AuNRT.[36,37] The resultant AuNRT exhibited narrow size distribution with an edge length of 34.9 ± 1.6 nm (n > 50) and side wall thickness of 3.9 ± 0.4 nm (n > 50) (Figure 1B). Extinction spectrum revealed the dipolar LSPR wavelength of the Au@Ag nanocubes at 434 nm. It is known that the LSPR wavelength of hollow plasmonic nanostructures, such as nanocages, and nanorattles is determined by the ratio of outer edge length to the wall thickness.[38] By controlling the volume of $HAuCl_4$ added to the template nanostructure solution during galvanic replacement reaction, the LSPR wavelength could be continuously shifted to longer wavelength.[39] In the present case, AuNRTs with an LSPR wavelength of ~700 nm were employed as nanotransducers.

The molecular imprinting on AuNRT involved multiple steps as depicted in Figure 1D and E. First, *p*-aminothiophenol (p-ATP) and glutaraldehyde (GA) were employed as the linker to immobilize template Hb on AuNRT by forming a reversible imine bond. Trimethoxysilane (TMPS) and (3-aminopropyl) trimethoxysilane (APTMS) were then copolymerized in the presence of template protein around the AuNRT. The methoxy group of the two monomers underwent a rapid hydrolysis and subsequent condensation to form an amorphous polymer matrix, leaving functional end groups ($-NH_3^+$, −OH, $-CH_3$) interacting with the target protein through electrostatic, hydrogen bonding, and hydrophobic interactions. Subsequently, bifunctional PEG (methoxy-PEG-silane) was covalently grafted to the free surface (i.e., regions not interacting with the template) of the siloxane copolymer. PEG chains were expected to shield various functional groups (NH_3^+, −OH, and $-CH_3$) of siloxane copolymer, thus negating nonspecific binding. The methoxysilane group of PEG underwent hydrolysis and then condensation with the reactive silanol (Si−OH) group present on the polymer surface to form a stable covalent siloxane bond (Si−O−Si) (Figure 1D). The target template protein was then removed by treating the molecular imprints with oxalic acid and sodium dodecyl sulfate (SDS), which broke the imine bond and overcame noncovalent interactions, respectively. Following the template protein removal, the AuNRT were left with siloxane copolymer coating with cavities complementary in shape and chemical functionality to the template protein. Each step described above was monitored by UV−vis extinction spectrum (described in detail later).

We have employed a series of surface characterization techniques to confirm the PEGylation of the molecular imprints. Chemical grafting of PEG chains to siloxane

DOI: 10.1021/acsami.6b07252
ACS Appl. Mater. Interfaces XXXX, XXX, XXX−XXX

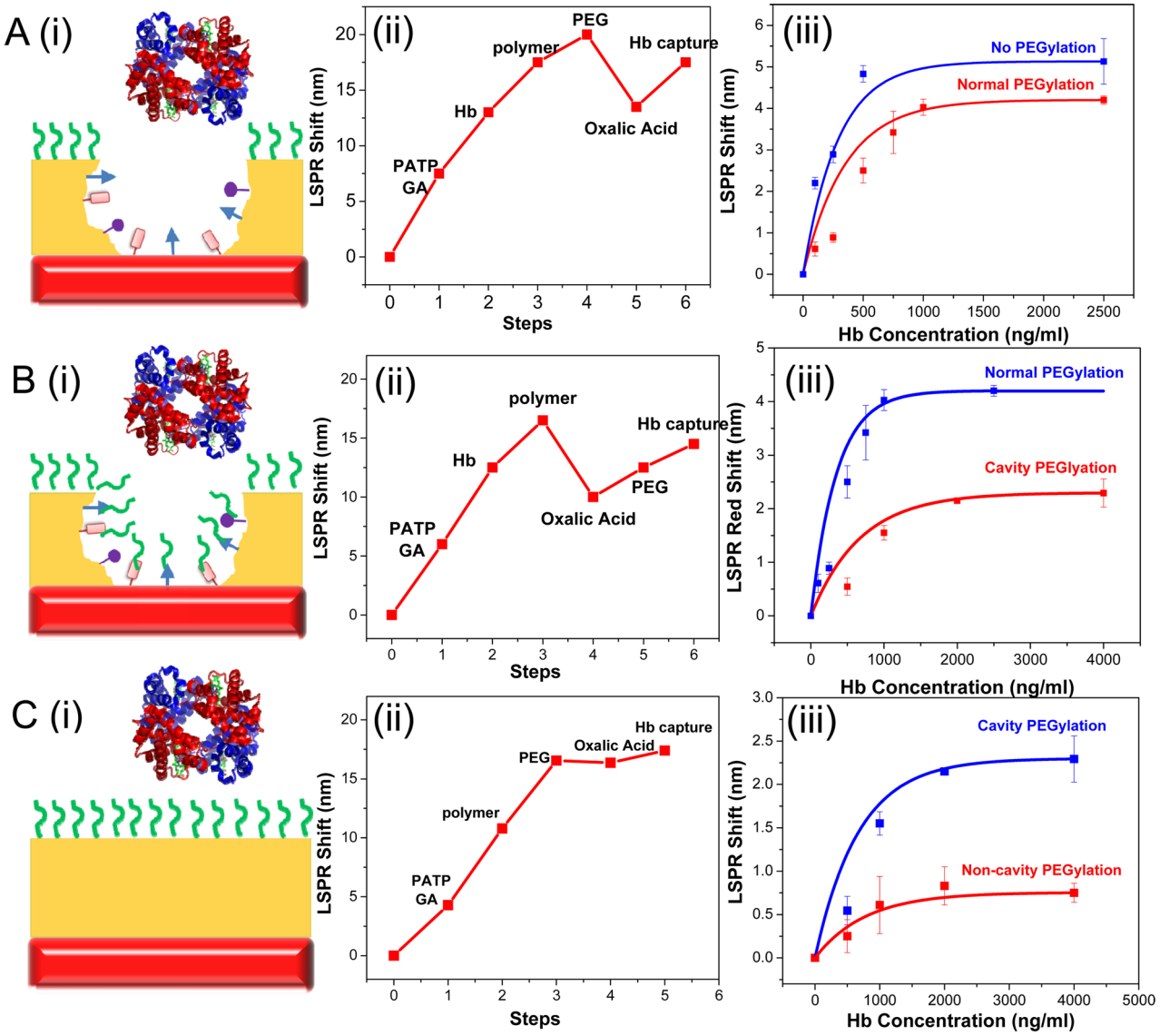

Figure 3. (A) PEGylation of molecular imprinted polymer before template removal: (i) schematic showing the PEGylated noncavity regions; (ii) LSPR shift of AuNRT after each step along the formation of the artificial antibodies, PEGylation, template removal, and template rebinding; (iii) plot showing the LSPR shift for various concentrations of Hb (target biomarker) with and without PEGylation. (B) PEGylation of molecular imprinted polymer after template removal: (i) schematic showing the PEGylated cavity and noncavity regions; (ii) LSPR shift of AuNRT after each step along the formation of the artificial antibodies, template removal, PEGylation, and template rebinding; (iii) plot showing the LSPR shift for various concentrations of Hb for artificial antibodies PEGylated before and after template removal; (C) PEGylation of siloxane copolymer without template: (i) schematic showing the PEGylated siloxane copolymer; (ii) LSPR shift of AuNRT after each step along the formation of siloxane copolymer on AuNRT, PEGylation, and nonspecific binding of proteins; (iii) plot showing the LSPR shift for various concentrations of Hb for PEGylated siloxane copolymer with and without recognition cavities.

copolymer surface is expected to result in an increase in the refractive index of the dielectric medium surrounding AuNRT. The refractive index increase upon PEGylation is evidenced by ~2.5 nm red shift in LSPR wavelength of AuNRT (Figure 2A). PEG is known to be highly hydrophilic and grafting PEG chains to the siloxane copolymer was expected to result in improved hydrophilicity of the siloxane surface and a decrease in the contact angle of water. The contact angle of siloxane copolymer layer deposited on flat silicon substrate was found to progressively decrease with an increase in the reaction time (see Experimental for details, Figure S2). The decrease in the contact angle from ~98° to ~69° indicated the successful modification of siloxane surface with hydrophilic PEG chains. Fourier transform infrared (FTIR) spectrum of PEGylated siloxane copolymer exhibited strong bands at 1106 and 2948 cm^{-1}, corresponding to C−O−C stretching and − CH_2 stretching vibrations, respectively, which are also indicative of successful PEGylation of the surface (Figure 2B). Finally, X-ray photoelectron spectroscopy (XPS) was employed to monitor the changes in the chemical functionality at the surface of siloxane copolymer after PEGylation. Quantitative insight was obtained from C 1s peak by using curve fitting software to calculate the relative contribution of two peaks corresponding to C−C (282.5 eV) and C−O (283.1 eV) to the total carbon concentration. A significant increase in the ratio of areas under C−O peak and C−C peak from 0.36 to 0.68 confirmed the successful grafting of the PEG chains to siloxane copolymer surface (Figure 2C and D).[40]

DOI: 10.1021/acsami.6b07252
ACS Appl. Mater. Interfaces XXXX, XXX, XXX−XXX

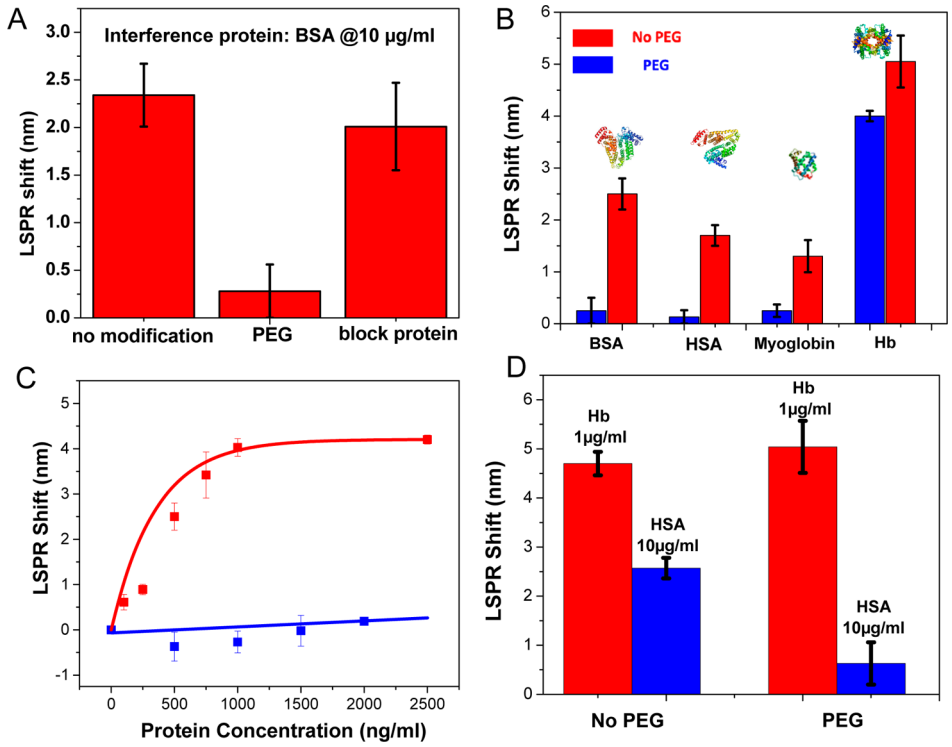

Figure 4. (A) Efficiency of different blocking methods in resisting the nonspecific adsorption of BSA (an interfering protein) on MIP. (B) LSPR shift of PEGylated and non-PEGylated MIPs on AuNRT after exposure to various interfering proteins (blue and red column for PEGylated, no PEGylation, respectively). (C) LSPR shift vs concentration of target (Hb) and interfering protein (HSA) depicting the excellent selectivity of the Hb-imprinted PEGylated artificial antibody. (D) Improved selectivity of PEGylated plasmonic biosensor to target biomarker (Hb) from artificial urine spiked with Hb (1 μg/mL) and HSA (10 μg/mL).

Now we turn our attention to the sensitivity of Hb plasmonic biosensor based on PEGylated molecular imprints. As noted above, PEG chains are grafted to the siloxane copolymer before removing the template biomolecules, which leaves the chemical functionality of the cavities intact (Figure 3A, (i)). Each step in the molecular imprinting process was monitored by following the LSPR shift of AuNRT (Figure 3A, (ii)). The accumulated red shift following various steps of imprinting process was found to be ~20 nm followed by a ~6 nm blue shift upon template protein extraction (Figure 3A, (ii)). The sensitivity of imprinted and PEGylated AuNRT was monitored by exposing them to different concentrations of Hb. For concentrations below 500 ng/mL, a monotonic increase in the LSPR shift of AuNRT was observed with increasing concentrations of Hb (Figure 3A, (iii)). The LSPR shift reached a plateau for concentrations higher than 500 ng/mL, indicating the saturation of the artificial antibodies with the target protein. To understand the influence of the PEGylation procedure, we have investigated the sensitivity of non-PEGylated imprinted AuNRT, which exhibited a similar trend i.e., progressive increase in the LSPR shift followed by saturation for higher concentrations. However, non-PEGylated imprinted AuNRT exhibited slightly higher LSPR shift at the same concentration of Hb compared to PEGylated imprinted AuNRT (Figure 3A, (iii)). The higher LSPR shift of non-PEGylated AuNRT can be ascribed to the higher nonspecific binding of the target protein to the noncavity regions of siloxane copolymer with abundant functional groups.[41]

Biorecognition of artificial antibodies is ascribed to complementarity of both shape and chemical functionality of the imprints to the target biomolecule.[42] As such, one should expect lower recognition and sensitivity if either one is perturbed or excluded. PEGylation of the siloxane copolymer layer after removing the template biomolecule should result in the passivation of both cavity and noncavity regions (Figure 3B, (i)). LSPR shifts after each imprinting step, including the PEGylation after template removal, are depicted in Figure 3B, (ii). For the same concentration of the target biomolecule, the LSPR shift of fully PEGylated AuNRT was found to be significantly lower compared to AuNRT with only the noncavity regions PEGylated (Figure 3B, (iii)). The significant decrease in the sensitivity of fully PEGylated AuNRT can be ascribed to (i) passivation of the entire surface with PEG chains that resist both specific (within the cavities) and nonspecific binding (outside the cavities) of the proteins; and (ii) perturbation of the shape of the recognition cavities due to the grafting of the polymer chains within the cavities. The residual capturing ability and sensitivity of the cavity PEGylated plasmonic biosensor could be attributed to the partial preservation of cavity shape.

As yet another control experiment, we tested the sensitivity of AuNRT that underwent all molecular imprinting steps without template proteins and full PEGylation of the siloxane layer (Figure 3C, (i)). LSPR shifts after various fabrication steps are depicted in Figure 3C, (ii). Notably, the PEGylation process resulted in a shift of around ~5 nm, which is considerably higher than the usual ~2.5 nm. It is known that the sensitivity of the plasmonic nanotransducer decays exponentially from the surface and the higher shift in the absence of template proteins is due to the proximity of the PEG chains to the plasmonic nanotransducer surface. An extremely small blue shift (less than 0.5 nm) was detected after exposure

DOI: 10.1021/acsami.6b07252
ACS Appl. Mater. Interfaces XXXX, XXX, XXX−XXX

to oxalic acid and SDS (employed for template protein removal), indicating the absence of significant desorption of PEG chains from the siloxane copolymer surface under these conditions (Figure 3C, (ii)). Not surprisingly, in the absence of cavity and fully PEGylated state, the AuNRT exhibited very limited target capturing ability and the LSPR shift saturated at ~0.5 nm. Compared to AuNRT with PEGylated cavities, PEGylated AuNRT with no cavities exhibited a huge decrease in the sensitivity and virtually complete loss of recognition capabilities. Taken together, these results clearly demonstrate the importance of complementary shape and chemical functionality of the molecular imprints for the capture of target proteins and in maximizing the sensitivity of plasmonic biosensors with artificial antibodies (Figure S3). These results also clearly highlight the importance of PEGylation of the siloxane copolymer layer before removing the template biomolecule.

We further investigated the ability of PEGylated artificial antibodies to resist nonspecific binding using representative interfering proteins. LSPR shift of Hb imprinted AuNRT upon exposure to interfering proteins was employed to quantify the nonspecific binding. Non-PEGylated and PEGylated AuNRT imprinted with Hb templates were exposed to bovine serum albumin (BSA) at a concentration of 10 μg/mL; a concentration equivalent to that of human serum albumin found in human urine (normal urine protein <20 μg/mL[43]). While non-PEGylated AuNRTs with artificial antibodies exhibited a LSPR shift of ~2.3 nm, PEGylated counterparts exhibited a LSPR shift of less than 0.3 nm (Figure 4A). The significantly lower LSPR shift of the PEGylated imprinted AuNRT indicates the excellent resistance to nonspecific binding. Passivation of noncavity regions using commercial blocking buffer (SuperBlock) did not significantly improve the resistance to nonspecific binding compared to non-PEGylated molecular imprints. In fact, we noted that the block proteins adsorbed on the noncavity regions of the siloxane copolymer are dislodged from the surface during template extraction step (oxalic acid plus SDS washing) as evidenced by the large blue shift (17 nm) compared to template protein extraction (7 nm) after PEGylation (see SI, Figure S4).

To further demonstrate the improved selectivity, plasmonic biosensors based on PEGylated molecular imprints were exposed to two other urinary proteins, namely, human serum albumin (HSA) and myoglobin (Mb) at a concentration of 10 μg/mL. The two proteins exhibited different molecular weight and isoelectric points compared to Hb. As mentioned above, albumin is present in human urine. Myoglobin is a particularly challenging candidate as interfering protein for Hb imprints considering the smaller size of Mb (Mw ~17.5 kDa) compared to Hb (Mw ~64 kDa), which can readily access the imprint cavities but not normally present in urine. Additionally, myoglobin can be considered tantamount to a monomer of hemoglobin possessing similar secondary and tertiary structure to hemoglobin α and β subunits. Myoglobinuria is problematic in rhabdomyolysis due to a number of pathologic conditions and due to crush injury.[44] Concentrations of 10 μg/mL myoglobin in urine are within the pathologic range contributing to kidney injury in humans.[44] Compared to non-PEGylated nanostructures, the PEGylated AuNRT imprinted with Hb, showed excellent resistance to (nonbinding of) both HSA and Mb (Figure 4B). The LSPR shift corresponding to nonspecific binding of HSA and Mb dropped from ~1.9 nm to ~0.2 nm and from ~1.5 nm to ~0.3 nm, respectively. Overall, the LSPR shift corresponding to the nonspecific binding of interfering protein at a concentration of 10 μg/mL was found to be nearly 20 times lower compared to that observed for Hb (target biomolecule) at a concentration of 1 μg/mL. To further evaluate nonspecific binding, the LSPR caused by HSA was examined at several concentrations. The LSPR shift for HSA (nonspecific) was found to be significantly lower compared to Hb (specific) over a broad concentration range (Figure 4C). In fact, at relatively low concentrations of HSA, we observed a small blue shift in the LSPR wavelength probably due to a small loss of organic material (e.g., loosely cross-linked siloxane copolymer) during the incubation of the plasmonic chip in the interfering protein solution for extended durations (Figure 4C).

Finally, PEGylated and non-PEGylated AuNRT imprinted with Hb were exposed to artificial urine samples spiked with Hb (1 μg/mL). Both PEGylated and non-PEGylated AuNRT exhibited large LSRR shifts (~5 nm) indicating the successful recognition and capture of the target biomolecule. Conversely, when exposed to synthetic urine spiked with HSA, the non-PEGylated AuNRT exhibited a relatively large LSPR shift of ~2.5 nm compared to PEGylated AuNRT that exhibited a shift of ~0.5 nm (Figure 4D). The significantly lower LSPR shift of PEGylated AuNRT compared to non-PEGylated counterparts signifies the large reduction in the nonspecific binding of albumin even from complex chemical matrix (i.e., synthetic urine), taking biosensors based on artificial antibodies closer to real-world applications.

3. CONCLUSIONS

To summarize, we demonstrated PEGylation of the non-recognition (i.e., noncavity) regions of the molecular imprints as a highly efficient and broadly applicable method to reduce nonspecific binding and significantly improve the selectivity of artificial antibodies. The LSPR shift due to non-specific binding on the PEGylated AuNRT was found to be nearly 10 times smaller than the non-PEGylated counterparts. Through a series of control experiments, we also demonstrated that the PEGylation process should precede template extraction to preserve the biorecognition capabilities of the molecular imprints. By simply changing the end functionality of the PEG chains, the approach demonstrated here can be broadly applied to a variety of monomers (e.g., acrylamides, acrylates) employed for molecular imprinting. The method demonstrated here can further be broadly applied for molecularly imprinted polymers employed in chromatography, electrophoresis, drug delivery, and biomimetic antibodies.

4. MATERIALS AND METHODS

Materials. Poly(ethylene glycol (PEG, Mw = 5000 g/mol) was obtained from JenKem Technology USA, MPTES ((3-Mercaptopropyl)triethoxysilane), cetyltrimethylammonium bromide (CTAB), cetyltrimethylammonium chloride(CTAC), ascorbic acid, sodium borohydride ($NaBH_4$), silver nitrate (purity >99%), 4-aminothiophenol (pATP), glutaraldehyde (GA), chloroauric acid ($HAuCl_4$), myoglobin from human heart (Mw = 17.7 kDa), albumin from bovine serum (Mw = 66.5 kDa), albumin from human serum (Mw = 65 kDa), and hemoglobin (Mw = 64.5 kDa) were obtained from Sigma-Aldrich. All the chemicals have been used as received with no further purification. The protein blocking solution (Odyssey Blocking Buffer (PBS)) was purchased from LI-COR Biosciences, Lincoln, NE.

Synthesis of Au Nanospheres. Au nanospheres were grown by seed-mediated method. First, Au seeds were synthesized by adding 0.6 mL of ice-cold $NaBH_4$ solution (10 mM) into a solution containing

DOI: 10.1021/acsami.6b07252
ACS Appl. Mater. Interfaces XXXX, XXX, XXX−XXX

0.25 mL $HAuCl_4$ (10 mM) and 9.75 mL CTAB (0.1 M) under vigorous stirring at room temperature for 10 min. The color of solution changed from yellow to brown indicating the formation of Au seed. This solution was kept undisturbed at room temperature for 3 h. Growth solution was prepared by mixing 6 mL of $HAuCl_4$ (0.5 mM) and 6 mL of CTAC (0.2 M) under stirring followed by the addition of 4.5 mL of ascorbic acid (100 mM). Subsequently, 0.3 mL of Au seed solution was added to the growth solution under stirring for 5 min. The growth solution was left undisturbed for 20 min to result in the formation of the Au nanospheres. Au nanospheres were centrifuged and redispersed in nanopure water for further use.

Synthesis of Au@Ag Nanocubes and Au Nanorattles. Au nanospheres (0.2 mL) and 4.8 mL of CTAC (20 mM) were mixed under stirring at 60 °C for 20 min. Subsequently, 5 mL of $AgNO_3$ (2 mM), 2.5 mL of CTAC (80 mM), and 2.5 mL of ascorbic acid (100 mM) were added under stirring at 60 °C, and the solution was further stirred for 4 h. After 4 h, the as-synthesized Au@Ag nanocubes were centrifuged (10 000 rpm for 15 min) and redispersed into a 15 mL aqueous solution of CTAC (50 mM). In order to synthesize AuNRT, $HAuCl_4$ aqueous solution (0.5 mM) was injected into the Au@Ag nanocube solution (0.5 mL/min) under stirring at 90 °C until the solution turned to blue color. The AuNRT solution was centrifuged at 10 000 rpm for 15 min and dispersed in nanopure water.

Absorption of AuNRTs on Glass Surface. Glass substrates employed for adsorbing AuNRTs were cleaned using Piranha solution (3:1 concentrated sulfuric acid to 30% hydrogen peroxide solution) followed by thorough rinsing with nanopure water (*Caution: Piranha solution is extremely dangerous and proper care needs to be executed in handling and disposal*). Cleaned glass substrates were immersed in 1% (v/v) MPTES in ethanol for 1 h followed by sonication for 30 min. Then the substrate was rinsed with ethanol and nanopure water. After drying the substrates under a stream of dry nitrogen, they were exposed to low concentration (absorbance adjusted to 0.2) of AuNRT solution for overnight (3 μL of HCl (1 M) was added to 1 mL AuNRT solution to facilitate adsorption). Finally, the substrate was rinsed with nanopure water to remove the loosely bound nanostructures, leaving uniformly coated AuNRTs on the glass substrate.

Molecular Imprinting and PEGylation Procedure. First, AuNRT adsorbed glass substrate was placed into 1 mL of $NaBH_4$ (100 mM) aqueous solution for 10 min with gentle shaking to remove CTAC from AuNRT surface, followed by thorough rinsing with nanopure water. Subsequently, the substrate were immersed into 2 mL of phosphate buffer (pH 8.0) containing 4 μL of glutaraldehyde (25%) and 4 μL of pATP (4 mM in ethanol) for 1 min, followed by rinsing with 0.01 mM phosphate buffered saline (PBS) pH 8.0 buffer. In the next step, template protein (Hb) was immobilized on AuNRT by exposing the substrate to 25 μg/mL of Hb in the pH 8.0 buffer at 4 °C for 2.5 h, followed by rinsing with pH 8.0 buffer solution. Five micorliters of TMPS and 5 μL of APTMS were added to 3 mL of 0.01 mM PBS pH 7.5 and the solution was thoroughly mixed. AuNRT modified glass substrate was then placed in the above silane mixture for 10 min to form the siloxane copolymer layer. After rinsing with nanopure water and drying under a stream of nitrogen, the substrate was immersed in 2 mg/mL PEG solution (in ethanol) for 8 h followed by thorough rinsing with ethanol and nanopure water. Finally, proteins were released by shaking the substrate in 1 mL of oxalic acid (10 mM) pH ∼ 2.3 in 2% aqueous sodium dodecyl sulfate (SDS) solution for 1 h.

Fabrication of Protein Blocked MIP Biosensor. After the polymerization step described above, the substrate was rinsed in PBS buffer pH ∼ 7.4 and then immersed in protein containing blocking buffer for overnight. The template on the substrate was released by shaking the substrate in 1 mL of oxalic acid (10 mM) in 2% aqueous SDS solution for 1 h.

Hb Detection and Interfering Proteins Test. After removing template proteins, the molecularly imprinted AuNRT biosensor on glass substrates were immersed in 1 mL of different concentrations of Hb in the pH 8.0 PBS buffer solution, followed by gently shaking for 30 min and then incubation at 4 °C for 3.5 h. The sample was then rinsed with nanopure water. UV−vis spectrum was obtained before and after the capture of the protein. The same procedure was employed for interfering proteins, including myoglobin from human heart (10 μg/mL), albumin from human serum (10 μg/mL), and albumin from bovine serum (10 μg/mL). The LSPR bands were fit using Gaussian peak fitting in order to determine the peak position. All measurements were performed in triplicates.

Selectivity Test in Artificial Urine. The artificial urine was spiked with Hb and HSA to achieve a final concentration of 1 μg/mL for Hb and 10 μg/mL for HSA. The protein spiked artificial urine solutions were applied to both PEGylated and non-PEGylated AuNRT samples by using the detection procedure described above.

Characterization. Transmission electron microscopy (TEM) micrographs were recorded on a JEM-2100F (JEOL) field emission instrument operating at an accelerating voltage of 200 kV. Samples were prepared by drying a drop of the solution on a carbon-coated grid, which had been previously made hydrophilic by glow discharge. Fourier transform infrared spectrometer (FTIR) spectra were recorded using a Nicolette Nexus 470 spectrometer. XPS analysis was performed using Physical Electronics 5000 VersaProbe II Scanning ESCA (XPS) Microprobe. The synthesis, deposition, functionalization, and protein binding detection of AuNRT were monitored through their vis-NIR extinction spectra collected using a Shimadzu 1800 spectrophotometer.

■ ASSOCIATED CONTENT

Ⓢ Supporting Information

The Supporting Information is available free of charge on the ACS Publications website at DOI: 10.1021/acsami.6b07252.

TEM image and UV−vis spectrum of the seed for AuNRT; change in the contact angle of siloxane copolymer with PEGylation reaction time; LSPR shift at each step along the molecular imprinting process using commercial block protein (PDF)

■ AUTHOR INFORMATION

Corresponding Author

*singamaneni@wustl.edu.

Notes

The authors declare no competing financial interest.

■ ACKNOWLEDGMENTS

We acknowledge support from National Science Foundation (CBET1254399) and National Institutes of Health (R21DK100759 and R01 CA141521). The authors thank Prof. Young-Shin Jun from the Department of Energy, Environmental and Chemical Engineering at Washington University for providing access to contact angle measurements, and Nano Research Facility (NRF) at Washington University for providing access to electron microscopy facilities.

■ REFERENCES

(1) Luong, J. H.; Male, K. B.; Glennon, J. D. Biosensor Technology: Technology Push versus Market Pull. *Biotechnol. Adv.* **2008**, *26* (5), 492−500.

(2) Stefan, R.-I.; Van Staden, J.; Aboul-Enein, H. Y. Immunosensors in Clinical Analysis. *Fresenius' J. Anal. Chem.* **2000**, *366* (6−7), 659−668.

(3) Wang, C.; Luan, J.; Tadepalli, S.; Liu, K.-K.; Morrissey, J. J.; Kharasch, E. D.; Naik, R. R.; Singamaneni, S. Silk-Encapsulated Plasmonic Biochips with Enhanced Thermal Stability. *ACS Appl. Mater. Interfaces* **2016**, DOI: 10.1021/acsami.6b07362.

(4) Tadepalli, S.; Kuang, Z.; Jiang, Q.; Liu, K.-K.; Fisher, M. A.; Morrissey, J. J.; Kharasch, E. D.; Slocik, J. M.; Naik, R. R.; Singamaneni, S. Peptide Functionalized Gold Nanorods for the

DOI: 10.1021/acsami.6b07252
ACS Appl. Mater. Interfaces XXXX, XXX, XXX−XXX

Sensitive Detection of a Cardiac Biomarker Using Plasmonic Paper Devices. *Sci. Rep.* **2015**, *5*, 16206.
(5) Chen, H.; Kou, X.; Yang, Z.; Ni, W.; Wang, J. Shape-and Size-dependent Refractive Index Sensitivity of Gold Nanoparticles. *Langmuir* **2008**, *24* (10), 5233−5237.
(6) Anker, J. N.; Hall, W. P.; Lyandres, O.; Shah, N. C.; Zhao, J.; Van Duyne, R. P. Biosensing with Plasmonic Nanosensors. *Nat. Mater.* **2008**, *7* (6), 442−453.
(7) Willets, K. A.; Van Duyne, R. P. Localized Surface Plasmon Resonance Spectroscopy and Sensing. *Annu. Rev. Phys. Chem.* **2007**, *58*, 267−297.
(8) Stewart, M. E.; Anderton, C. R.; Thompson, L. B.; Maria, J.; Gray, S. K.; Rogers, J.; Nuzzo, R. Nanostructured Plasmonic Sensors. *Chem. Rev.* **2008**, *108* (2), 494−521.
(9) Mayer, K. M.; Hafner, J. H. Localized Surface Plasmon Resonance Sensors. *Chem. Rev.* **2011**, *111* (6), 3828−3857.
(10) Mosbach, K.; Ramström, O. The Emerging Technique of Molecular Imprinting and its Future Impact of Biotechnology. *Bio/Technology* **1996**, *14* (2), 163−170.
(11) Haupt, K.; Mosbach, K. Molecularly Imprinted Polymers and their Use in Biomimetic Sensors. *Chem. Rev.* **2000**, *100* (7), 2495−2504.
(12) Wulff, G. Molecular Imprinting in Cross-linked Materials with the Aid of Molecular Templates—a Way towards Artificial Antibodies. *Angew. Chem., Int. Ed. Engl.* **1995**, *34* (17), 1812−1832.
(13) Dutta, P.; Pernites, R. B.; Danda, C.; Advincula, R. C. SPR Detection of Dopamine Using Cathodically Electropolymerized, Molecularly Imprinted Poly-p-aminostyrene Thin Films. *Macromol. Chem. Phys.* **2011**, *212* (22), 2439−2451.
(14) Cai, D.; Ren, L.; Zhao, H.; Xu, C.; Zhang, L.; Yu, Y.; Wang, H.; Lan, Y.; Roberts, M. F.; Chuang, J. H.; et al. A Molecular-imprint Nanosensor for Ultrasensitive Detection of Proteins. *Nat. Nanotechnol.* **2010**, *5* (8), 597−601.
(15) Haupt, K. Biomaterials: Plastic Antibodies. *Nat. Mater.* **2010**, *9* (8), 612−614.
(16) Bui, B. T. S.; Haupt, K. Molecularly Imprinted Polymers: Synthetic Receptors in Bioanalysis. *Anal. Bioanal. Chem.* **2010**, *398* (6), 2481−2492.
(17) Abbas, A.; Tian, L.; Morrissey, J. J.; Kharasch, E. D.; Singamaneni, S. Hot Spot-Localized Artificial Antibodies for Label-Free Plasmonic Biosensing. *Adv. Funct. Mater.* **2013**, *23* (14), 1789−1797.
(18) Tian, L.; Liu, K.-K.; Morrissey, J. J.; Gandra, N.; Kharasch, E. D.; Singamaneni, S. Gold Nanocages with Built-in Artificial Antibodies for Label-free Plasmonic Biosensing. *J. Mater. Chem. B* **2014**, *2* (2), 167−170.
(19) Asanuma, H.; Hishiya, T.; Komiyama, M. Tailor-made Receptors by Molecular Imprinting. *Adv. Mater.* **2000**, *12* (14), 1019−1030.
(20) Komiyama, M.; Takeuchi, T.; Mukawa, T.; Asanuma, H. Front Matter. *Molecular Imprinting* **2002**, i−xii.
(21) Turner, N. W.; Jeans, C. W.; Brain, K. R.; Allender, C. J.; Hlady, V.; Britt, D. W. From 3D to 2D: a Review of the Molecular Imprinting of Proteins. *Biotechnol. Prog.* **2006**, *22* (6), 1474−1489.
(22) Hoshino, Y.; Kodama, T.; Okahata, Y.; Shea, K. J. Peptide Imprinted Polymer Nanoparticles: a Plastic Antibody. *J. Am. Chem. Soc.* **2008**, *130* (46), 15242−15243.
(23) Tov, O. Y.; Luvitch, S.; Bianco-Peled, H. Molecularly Imprinted Hydrogel Displaying Reduced Non-specific Binding and Improved Protein Recognition. *J. Sep. Sci.* **2010**, *33* (11), 1673−1681.
(24) Nishino, H.; Huang, C. S.; Shea, K. J. Selective Protein Capture by Epitope Imprinting. *Angew. Chem., Int. Ed.* **2006**, *45* (15), 2392−2396.
(25) Qian, X.; Peng, X.-H.; Ansari, D. O.; Yin-Goen, Q.; Chen, G. Z.; Shin, D. M.; Yang, L.; Young, A. N.; Wang, M. D.; Nie, S. In Vivo Tumor Targeting and Spectroscopic Detection with Surface-enhanced Raman Nanoparticle Tags. *Nat. Biotechnol.* **2007**, *26* (1), 83−90.
(26) Cheng, L.; Wang, C.; Feng, L.; Yang, K.; Liu, Z. Functional Nanomaterials for Phototherapies of Cancer. *Chem. Rev.* **2014**, *114* (21), 10869−10939.
(27) Pochechueva, T.; Chinarev, A.; Bovin, N.; Fedier, A.; Jacob, F.; Heinzelmann-Schwarz, V. PEGylation of Microbead Surfaces Reduces Unspecific Antibody Binding in Glycan-based Suspension Array. *J. Immunol. Methods* **2014**, *412*, 42−52.
(28) Sun, Y.; Mayers, B.; Xia, Y. Metal Nanostructures with Hollow Interiors. *Adv. Mater.* **2003**, *15* (7−8), 641−646.
(29) Morrissey, J. J.; Kharasch, E. D. The Specificity of Urinary Aquaporin 1 and Perilipin 2 to Screen for Renal Cell Carcinoma. *J. Urol.* **2013**, *189* (5), 1913−1920.
(30) Wong, E. K.; Goodship, T. H.; Kavanagh, D. Complement Therapy in Atypical Haemolytic Uraemic Syndrome (aHUS). *Mol. Immunol.* **2013**, *56* (3), 199−212.
(31) Hill, A.; Kelly, R. J.; Hillmen, P. Thrombosis in Paroxysmal Nocturnal Hemoglobinuria. *Blood* **2013**, *121* (25), 4985−4996.
(32) HAM, T. H. Studies on Destruction of Red Blood Cells: I. Chronic Hemolytic Anemia with Paroxysmal Nocturnal Hemoglobinuria: an Investigation of the Mechanism of Hemolysis, with Observations on Five Cases. *Arch Intern Med.* **1939**, *64* (6), 1271−1305.
(33) Zheng, Y.; Ma, Y.; Zeng, J.; Zhong, X.; Jin, M.; Li, Z.-Y.; Xia, Y. Seed-Mediated Synthesis of Single-Crystal Gold Nanospheres with Controlled Diameters in the Range 5−30 nm and their Self-Assembly upon Dilution. *Chem. - Asian J.* **2013**, *8* (4), 792−799.
(34) Ma, Y.; Li, W.; Cho, E. C.; Li, Z.; Yu, T.; Zeng, J.; Xie, Z.; Xia, Y. Au@Ag Core−Shell Nanocubes with Finely Tuned and Well-Controlled Sizes, Shell Thicknesses, and Optical Properties. *ACS Nano* **2010**, *4* (11), 6725−6734.
(35) Xia, X.; Wang, Y.; Ruditskiy, A.; Xia, Y. 25th Anniversary Article: Galvanic Replacement: A Simple and Versatile Route to Hollow Nanostructures with Tunable and Well-Controlled Properties. *Adv. Mater.* **2013**, *25* (44), 6313−6333.
(36) Sun, Y.; Mayers, B.; Xia, Y. Metal Nanostructures with Hollow Interiors. *Adv. Mater.* **2003**, *15* (7−8), 641−646.
(37) Gandra, N.; Portz, C.; Singamaneni, S. Biomedical Applications: Multifunctional Plasmonic Nanorattles for Spectrum-Guided Locoregional Therapy (Adv. Mater. 3/2014). *Adv. Mater.* **2014**, *26* (3), 350−350.
(38) Mahmoud, M. A.; El-Sayed, M. A. Gold Nanoframes: Very High Surface Plasmon Fields and Excellent Near-Infrared Sensors. *J. Am. Chem. Soc.* **2010**, *132* (36), 12704−12710.
(39) Xia, X.; Wang, Y.; Ruditskiy, A.; Xia, Y. 25th Anniversary Article: Galvanic Replacement: A Simple and Versatile Route to Hollow Nanostructures with Tunable and Well-Controlled Properties. *Adv. Mater.* **2013**, *25* (44), 6313−6333.
(40) Sharma, S.; Johnson, R. W.; Desai, T. A. XPS and AFM Analysis of Antifouling PEG Interfaces for Microfabricated Silicon Biosensors. *Biosens. Bioelectron.* **2004**, *20* (2), 227−239.
(41) Ross, P. D.; Subramanian, S. Thermodynamics of Protein Association Reactions: Forces Contributing to Stability. *Biochemistry* **1981**, *20* (11), 3096−3102.
(42) Cram, D. J. The Design of Molecular Hosts, Guests, and their Complexes (Nobel Lecture). *Angew. Chem., Int. Ed. Engl.* **1988**, *27* (8), 1009−1020.
(43) Levey, A. S.; Eckardt, K.-U.; Tsukamoto, Y.; Levin, A.; Coresh, J.; Rossert, J.; Zeeuw, D. D.; Hostetter, T. H.; Lameire, N.; Eknoyan, G. Definition and Classification of Chronic Kidney Disease: a Position Statement from Kidney Disease: Improving Global Outcomes (KDIGO). *Kidney Int.* **2005**, *67* (6), 2089−2100.
(44) Gibney, R. N.; Sever, M. S.; Vanholder, R. C. Disaster Nephrology: Crush Injury and Beyond. *Kidney Int.* **2014**, *85* (5), 1049−1057.

DOI: 10.1021/acsami.6b07252
ACS Appl. Mater. Interfaces XXXX, XXX, XXX−XXX